Bulletin of the Seismological Society of America, Vol. 99, No. 1, pp. 52–60, February 2009, doi: 10.1785/0120080005

# Spatiotemporal Complexity of Continental Intraplate Seismicity: Insights from Geodynamic Modeling and Implications for Seismic Hazard Estimation

by Qingsong Li, Mian Liu, and Seth Stein

Abstract Continental intraplate seismicity seems often episodic, clustered, and migrating. The observed seismicity shows both spatial clustering in seismic zones and scattering across large plate interiors, temporal clustering followed by long periods of quiescence, and migration of seismicity from one seismic zone to another. Here, we explore the complex spatiotemporal patterns of intraplate seismicity using a 3D visco-elasto-plastic finite-element model. The model simulates tectonic loading, crustal failure in earthquakes, and coseismic and postseismic stress evolution. For a laterally homogeneous lithosphere with randomly prespecified perturbations of crustal strength, the model predicts various spatiotemporal patterns of seismicity at different timescales: spatial clustering in narrow belts and scattering across large regions over hundreds of years, connected seismic belts over thousands of years, and widely scattered seismicity over tens of thousands of years. The orientation of seismic belts coincides with the optimal failure directions associated with the assumed tectonic loading. Stress triggering and migration cause spatiotemporal clustering of earthquakes. When weak zones are included in the model the predicted seismicity initiates within the weak zones but then extends far beyond them. If a fault zone is weakened following a large earthquake, repeated large earthquakes can occur on the same fault zone even in the absence of strong tectonic loading. These complex spatiotemporal patterns of intraplate seismicity predicted in this simple model suggest that assessment of earthquake hazard based on the limited historic record may be biased toward overestimating the hazard in regions of recent large earthquakes and underestimating the hazard where seismicity has been low during the historic record.

## Introduction

The distribution of earthquakes in space and time within continental interiors is far more complex than on major plate boundary faults. Earthquakes on plate boundaries result from strain produced by steady relative plate motions. Hence, plate boundaries remain the loci of large quasi-periodic earthquakes for long intervals until the plate boundary geometry changes. As a result, the long-term pattern of seismicity inferred from geological fault studies is generally consistent with that observed in large earthquakes in historic/instrumental records (e.g., Marco *et al.*, 1996; Weldon *et al.*, 2004; Cisternas *et al.*, 2005). Moreover, the direction and rate of geodetically observed strain accumulation is generally consistent with the mechanisms and recurrence of large earthquakes (Stein and Freymueller, 2002).

The situation is quite different within continental plate interiors, where earthquakes appear to be clustered, episodic, and migrating in space (Fig. 1). Paleoseismic data show that intraplate earthquakes often occur in temporal clusters on faults that remain active for some time and then have long quiescent periods during which other fault zones are active (Crone *et al.*, 2003; Camelbeeck *et al.*, 2007). Thus, some faults without historically recorded earthquakes, such as the Meers fault in Oklahoma (Crone and Luza, 1990), appear to have had prehistoric large events (Clark and McCue, 2003).

Besides individual faults, earthquakes in continental intraplate regions also appear to occur in temporal clusters. For example, earthquakes in North China's Weihe-Shanxi graben are temporally clustered before 1700 (Fig. 2a). Similarly, large earthquakes ($M > 6$) in the North China Plain are clustered between 1900 and 2000 (Fig. 2b). Moreover, the locus of seismicity seems to be migrating from the Weihe-Shanxi graben eastward to the North China Plain in the past 200 yr (Fig. 1b).

The spatial patterns of continental intraplate seismicity are also complex, with both spatial clustering of earthquakes in seismic zones and scattered activity over large regions

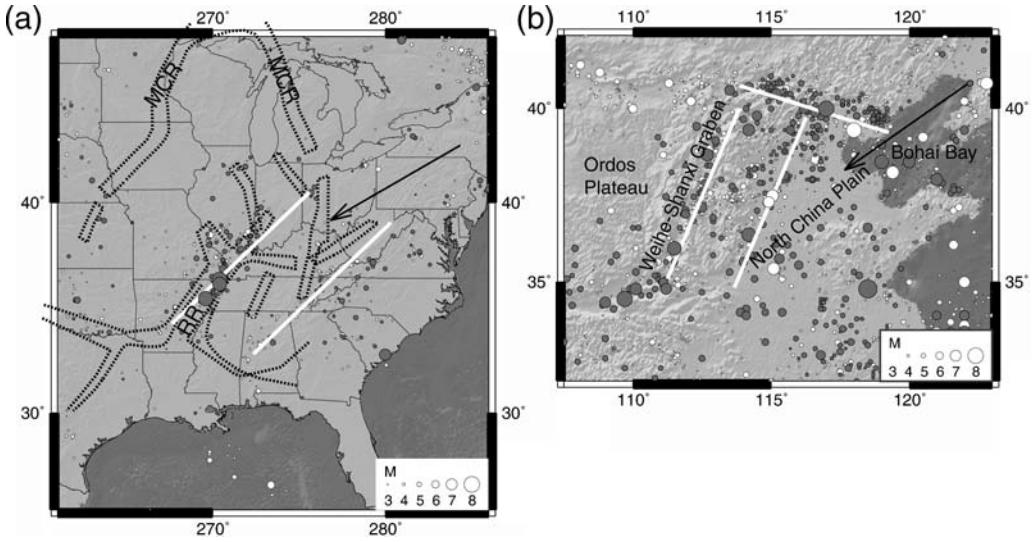


**Figure 1** Intracontinental earthquakes in (a) the CEUS and (b) North China. Dashed lines in (a) show the rift zones: midcontinent rift, MCR; and Reelfoot rift, RR. Data for the CEUS are from the National Earthquake Information Center (NEIC) catalog. Earthquake data of North China are from China Earthquake Administration. Gray dots in CEUS represent earthquakes before 1973; white dots represent earthquakes after 1973. Gray dots in North China represent earthquakes before 1900; white dots represent earthquakes after 1900. Thick lines are regional trends of seismic belts; black arrows are the direction of maximum compressive stress.

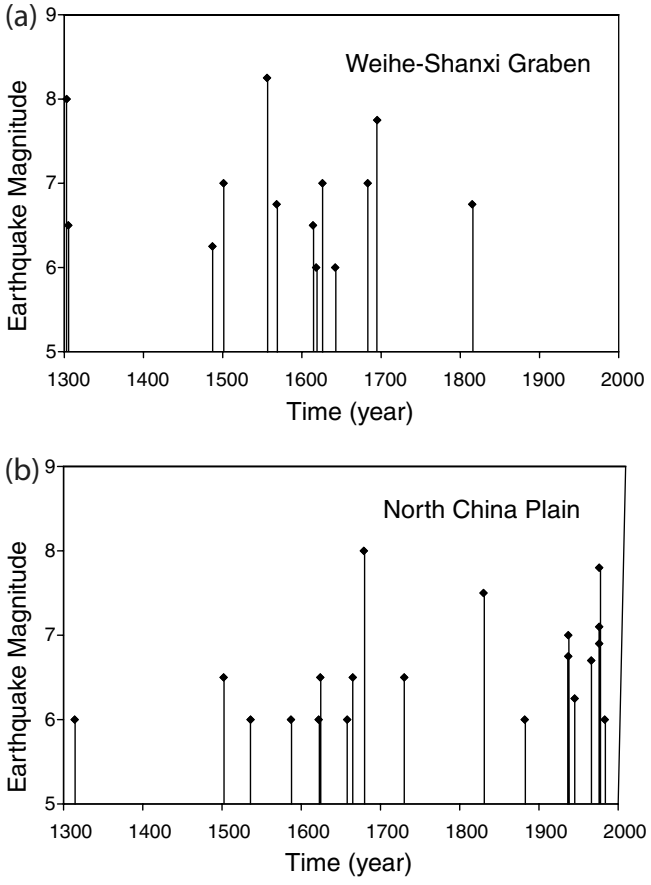


**Figure 2** Historic records of intraplate earthquakes ($M > 6$) in (a) the Weihe-Shanxi graben and (b) the North China Plain.

(Fig. 1). For example, historic and instrumentally recorded earthquakes in the central and eastern United States (CEUS) appear to be concentrated in several zones, notably the New Madrid, Charleston, and Eastern Tennessee seismic zones (Fig. 1a). In addition, scattered seismicity occurs outside these zones. Some seismic zones, such as the New Madrid zone, occur along the failed rift zones, but other seismic zones do not (Schulte and Mooney, 2005). Conversely, some prominent rifts, such as the midcontinent rift in central North America, have little seismicity (Fig. 1a). As a result, the relation between continental intraplate seismicity and geologic structure remains uncertain and the subject of active investigation, as summarized by papers in Stein and Mazzotti (2007).

The complex variation of seismicity in space and time poses a major challenge for seismic hazard estimation. It seems likely that inferring seismic hazards from historical seismicity can overestimate the hazard where recent earthquakes have occurred and underestimate the hazard elsewhere (e.g., Swafford and Stein, 2007; van Lanen and Mooney, 2007). To reduce this difficulty, researchers have developed hazard maps that also reflect geologic structure, yielding maps that predict more diffuse hazards (Halchuk and Adams, 1999; Tóth *et al.*, 2006).

Numerous models have attempted to explain the complexities of intraplate seismicity. Generally, these models involve temporal variations of the physical properties of faults and the stress acting on them. Crone *et al.* (2003) suggest that temporal clustering, in which faults turn on to generate a series of large earthquakes and then turn off for a long time, may reflect the evolution of pore fluid pressure in the fault zone (Sibson, 1992). In this model, low-permeability seals

form around the fault zone as stress accumulates, raising the pore pressure until an earthquake happens. Faults that weaken during earthquakes and heal during interseismic phases could also contribute to the complexity of seismicity (Lyakhovsky *et al.*, 2001). The migration of seismicity between faults may result from stress transfer, in which stress changes due to earthquakes affect the location of future events (Stein, 1999; Chéry *et al.*, 2001; Mueller *et al.*, 2004; Rundle *et al.*, 2006). Failure and viscous relaxation of the lower crust may cause a sequence of fault ruptures in short recurrence intervals (Kenner and Segall, 2000).

Most of these studies are focused on a single event or fault zone, and regional tectonic loading is often ignored (e.g., Kenner and Segall, 2000; Lyakhovsky *et al.*, 2001; Crone *et al.*, 2003). In this study we explore the complexity of intraplate earthquakes and some of the controlling factors in a regional scale finite-element model.

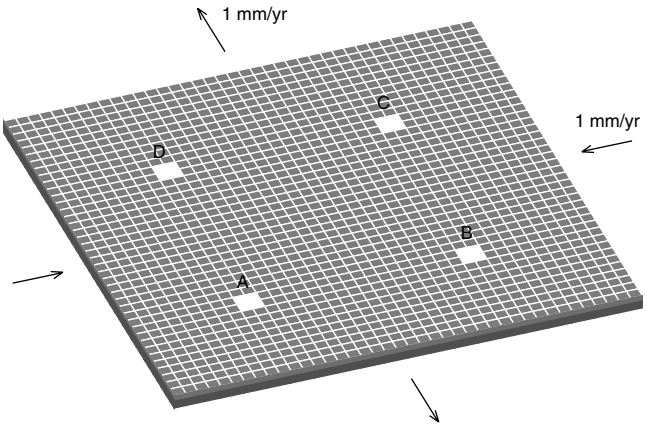


**Figure 3** Finite-element model for case 1. The model is loaded by compression at the eastern and western boundaries and by extension at the northern and southern boundaries. The light gray layer represents the brittle (elastoplastic) upper crust; the dark gray layer represents the ductile (viscoelastic) lower crust and upper mantle. A, B, C, and D are four small regions used for showing seismicity clustering in Figure 7.

## Finite-Element Model

Our model is built on the 3D visco-elasto-plastic finite-element model we developed for simulating lithosphere deformation (Li and Liu, 2006, 2007). The model simulates tectonic loading, crustal failure in earthquakes, and the associated coseismic and postseismic stress evolution. Tectonic loading is simulated by applying velocity boundary conditions at the model boundaries. Crustal failure in an earthquake is simulated by instantly decreasing strength in an element by a given amount when stress in the element reaches the Drucker–Prager failure criterion. The Drucker–Prager criterion is similar to the Mohr–Coulomb criterion but is more numerically stable. Stress drop at the failed element changes the stress in the surrounding elements. Further stress changes may derive from postseismic viscous relaxation of the lower crust and the upper mantle. The coseismic and postseismic stress changes in the elements that failed may increase (or decrease) stress in the neighboring regions, thus promoting (or inhibiting) earthquake occurrence there.

The model dimension is 2000 by 2000 km and is 60 km thick (Fig. 3). A 20 km thick elastoplastic upper layer simulates the brittle upper crust (the schizosphere) and a 40 km thick viscoelastic lower layer simulates the ductile lower crust and upper mantle (the plastosphere). Using different thickness of these layers within reasonable ranges does not affect the main model results. The eastern and western boundaries are compressed uniformly at 1 mm/yr, while the northern and southern boundaries are extended at the same rate. The resulting strain rate is $\sim 5.0 \times 10^{-10}$ yr$^{-1}$, typical for the deformation rate in continental intraplate regions (e.g., Newman *et al.*, 1999; Gan and Prescott, 2001; Calais *et al.*, 2005). The bottom boundary is free slip. Young's modulus is $8.75 \times 10^{10}$ Pa, and Poison's ratio is 0.25 for both the crust and the mantle (Turcotte and Schubert, 1982). For most cases we take the viscosity for the lower layer to be $1 \times 10^{20}$ Pa sec, which is within the range between the lower crust viscosity from postseismic deformation studies ($10^{19}$ Pa sec or less, e.g., Pollitz *et al.*, 2001a) and the viscosity from postglacial rebound studies ($\sim 10^{21}$ Pa sec, e.g., Hager, 1991). The yield strength of the upper layer is described by a value of 50 MPa for the cohesion and 0.4 for the coefficient of internal friction. These values are within the reasonable ranges for the upper crust and were used in previous modeling studies (e.g., Kenner and Segall, 2000). When crust fails, the stress drops by 1 MPa. The energy release is equivalent to an $M \sim 6$ earthquake for one failed element ($50 \times 50 \times 10$ km).

To minimize the impact of the poorly constrained initial stress state, we begin the numerical experiments after the model has reached a quasi-steady state. Figure 4 shows an example of how the predicted stress and earthquakes evolve. Figure 4a shows the stress at the beginning of a 1000 yr period to be examined; the black dots are the earthquakes that occurred during this period. Figure 4b shows the stress at the end of this 1000 yr period. The earthquakes occur within regions of high stresses. Each earthquake causes stress to drop below the crustal yield strength in the failed elements. The stress drop also perturbs stress in the neighboring. Hence, the stress field in the model domain continuously evolves with time.

## Model Results

To illustrate the effect of various factors on the predicted spatiotemporal patterns of intraplate seismicity, we start with a simple model with a horizontally homogeneous crust and mantle and then incrementally increase the model complexity.

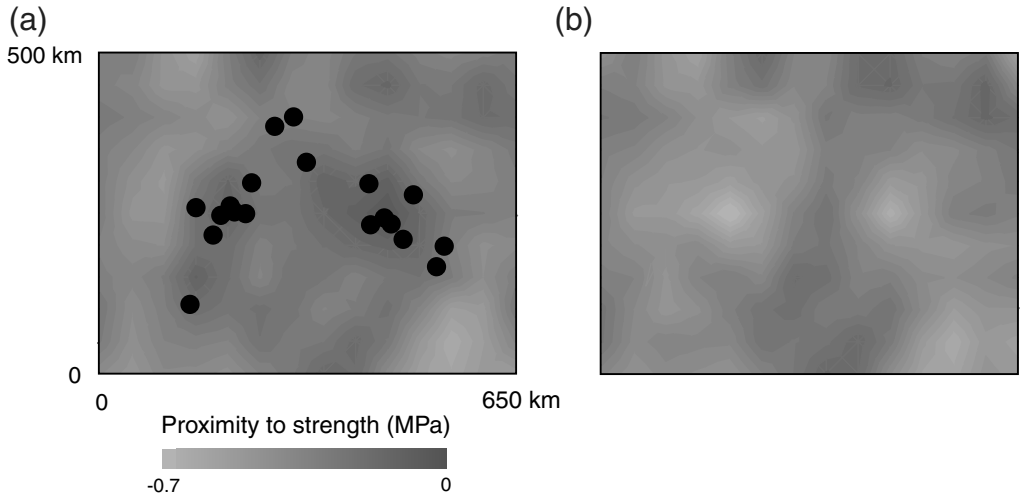


**Figure 4** Evolution of stress and seismicity over a 1000 yr period in the model. (a) Initial stress level: the gray scale indicates how close the stress is to the crustal yield strength. The dots are epicenters of predicted earthquakes in the following 1000 yr. (b) The stress level at the end of the 1000 yr period.

Case 1: Timescale-Dependent Spatiotemporal Patterns of Seismicity

In this case, a randomly prespecified perturbation of the crustal strength (Fig. 5), which is kept constant through the modeling, is applied to an otherwise laterally homogeneous crust and mantle (Fig. 3). The magnitude of the perturbation ranges from −0.5 to 0.5 MPa, which are small values compared with the crustal strength and stress drop in crustal failure events. To some extent, this perturbation simulates the lateral heterogeneity of the continental crust.

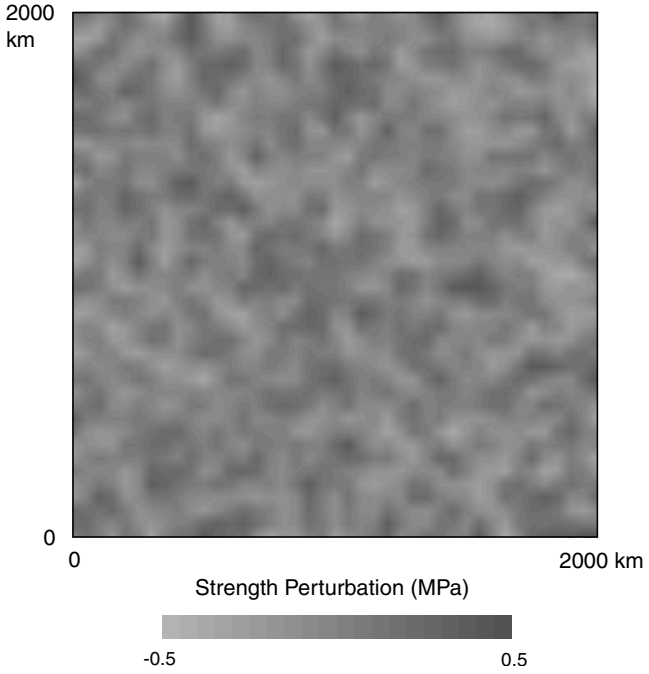


**Figure 5** The random crustal strength perturbation used in case 1.

The resulting seismicity shows both spatial clustering (in spots and belts) and scattering (over large regions) over a period of 300 yr (Fig. 6a). Over a longer period, 3000 yr, the earthquake clusters connect to form a network of seismic zones (Fig. 6b). Over an even longer time, 30,000 yr, seismicity covers the entire model domain (Fig. 6c). This result is expected because the model domain is horizontally homogeneous. Hence, seismicity is uniform over the long term but is concentrated in seismic zones during shorter intervals.

The model results also show temporal clustering of earthquakes in seismic zones. Figure 7 shows the predicted earthquake sequences for four 100 $km^2$ regions, each containing four finite-element cells. Temporal clustering of earthquakes occurs in region B between 10,000 and 20,000 yr and in region C around 5000 and 22,000 yr. The temporal clustering is caused by coseismic and postseismic stress triggering among the neighboring elements. Without coseismic and postseismic stress interaction between regions, we would expect periodic earthquake occurrence because the model has constant loading and constant stress release in earthquakes.

The orientations of the predicted seismic belts, northwest–southeast or northeast–southwest, coincide with the optimal failure directions (maximum shear stress) resulting from the boundary conditions of east–west compression and north–south extension.

Case 2: Effects of Weak Zones

In this case we replace the random perturbation of the initial crustal strength with three weak zones whose yield strength is 5 MPa lower than the rest of the model domain (Fig. 8a). Two of the zones are parallel to each other and

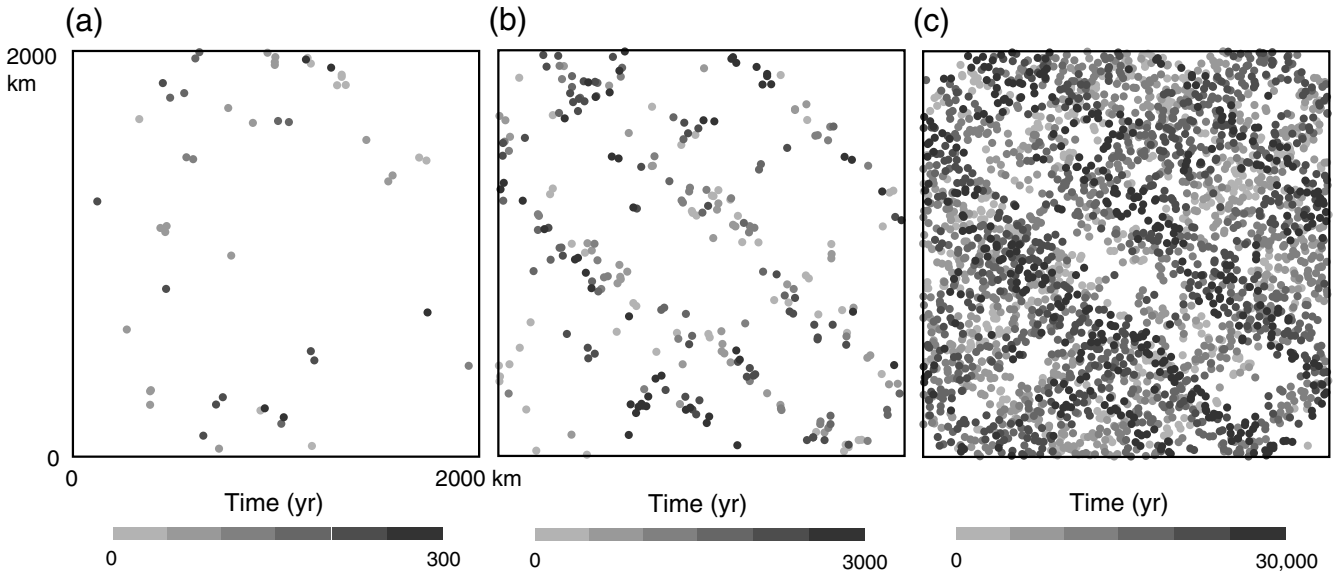


**Figure 6** Seismicity in case 1 that occurred over timescales of (a) 300 yr, (b) 3000 yr, and (c) 30,000 yr. The gray scale of dots represents the time within each of the three time intervals.

are perpendicular to the third. The initial stress is set to zero, and the model is constantly loaded at the boundaries. Initially earthquakes occur only within the weak zones. After ~80, 000 model years, stress in the surrounding crust begins to reach the strength and cause failure. After another 100,000 yr, model seismicity reaches a quasi-steady state, in which the predicted seismicity during one long period (> 60, 000 yr) is similar to another.

The spatiotemporal pattern of seismicity on different timescales is shown in Figure 8. On a short timescale (600 yr), earthquakes occur both inside and outside the weak zones (Fig. 8a). The seismicity shows some spatial clustering with no clear correlation with the weak zones. Over a longer period (6000 yr), the seismicity forms belts extending from the weak zone (Fig. 8b). This pattern remains the same over longer periods (Fig. 8c). Hence, on the long timescales, seis-

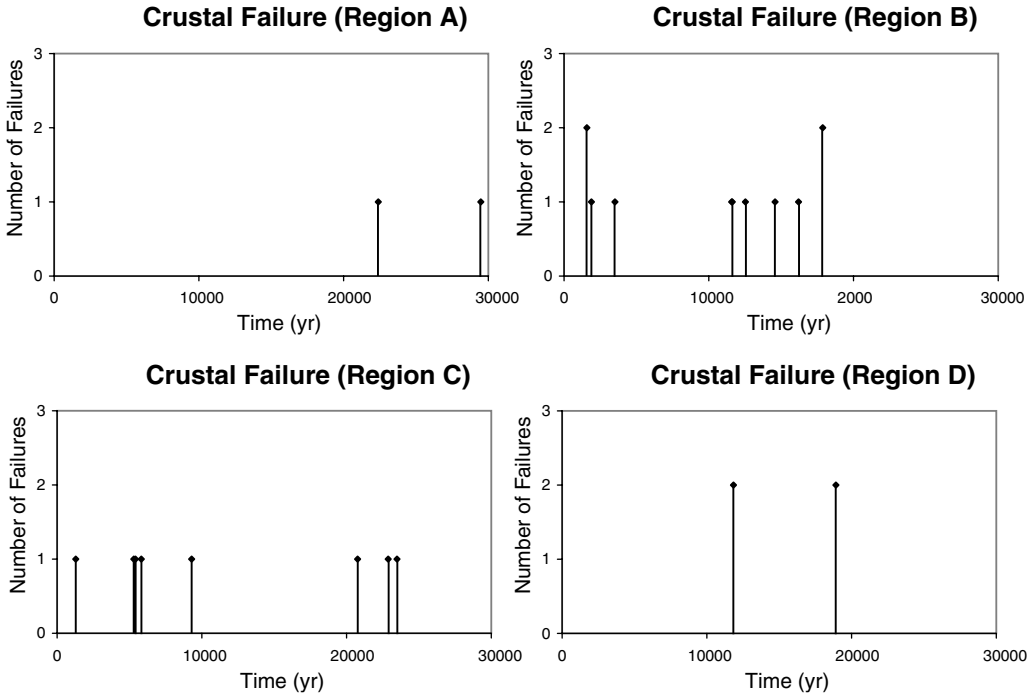


**Figure 7** Temporal distribution of predicted earthquakes in regions A, B, C, and D shown in Figure 3.

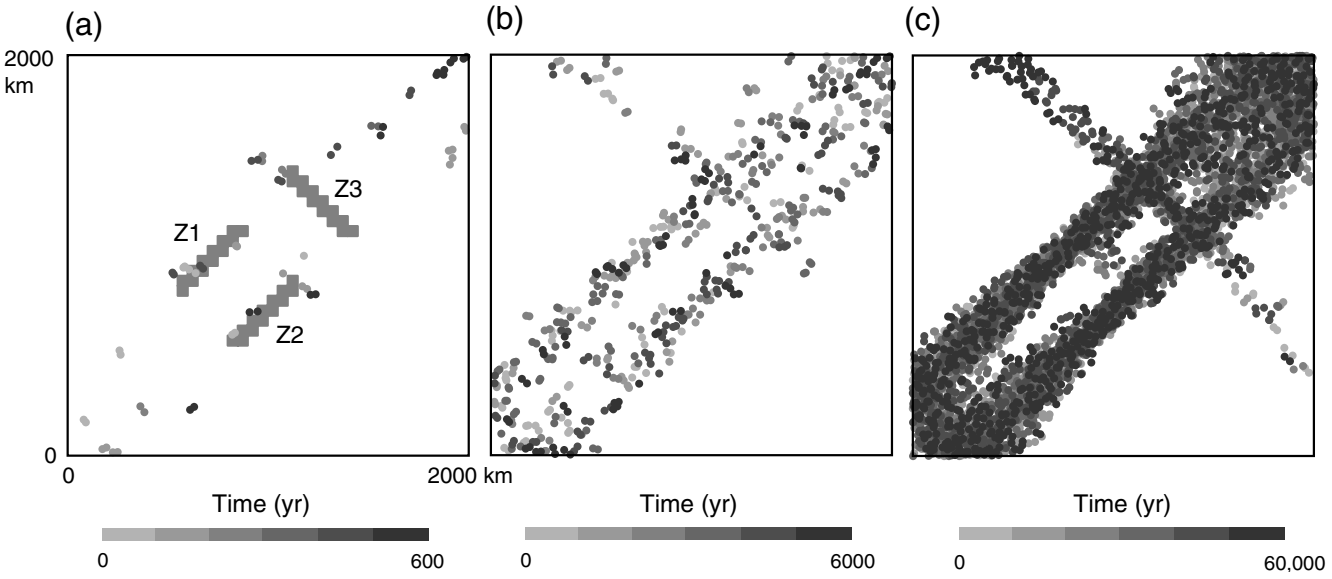


**Figure 8** Seismicity in case 2 that occurred over timescales of (a) 600 yr, (b) 6000 yr, and (c) 60,000 yr. The gray scale of dots represents the time within each of the three time intervals. The gray belts in (a) are prespecified weak zones.

micity is not confined to the weak zones. Moreover, as in the previous case, the short-term seismicity pattern does not fully represent that over longer terms.

Case 3: Effects of Fault Weakening

In the first two cases spatial variations in crustal strength cause the spatiotemporal variations in seismicity. In the third case we explore the effects of temporal variation in fault properties. In this case the crust has a uniform strength except along a single fault. This analysis is motivated by the fact that paleoearthquake and fault offset studies have found evidence of repeated ruptures on individual intraplate faults and fault zones in short periods followed by long periods of quiescence (Tuttle *et al.*, 2002; Crone *et al.*, 2003). The short time between the repeated earthquakes on these intraplate faults, such as the ~500 yr found for the recent large events in the New Madrid zone (Tuttle *et al.*, 2002), is at odds with the low rates of deformation and far-field loading in plate interiors (Newman *et al.*, 1999; Calais *et al.*, 2005). Li *et al.* (2005) have shown that a large intraplate earthquake can reduce stress in the fault zone such that thousands of years would be needed for stress to rebuild for another similar rupture. Thus, large intraplate earthquakes repeating in short time intervals would require either some kind of local loading to build up the stress or local weakening to permit repeated failure at lowered stress levels.

A number of mechanisms for local loading and/or fault weakening have been proposed (e.g., Kenner and Segall, 2000; Pollitz *et al.*, 2001b), although there is no direct evidence for the proposed weakening (McKenna *et al.*, 2007). Assuming some kind of fault weakening occurs in nature (Sibson, 1992; Lyakhovsky *et al.*, 2001), we explore here its effect on seismicity. In this case we explicitly incorporate a weak fault zone (zone Z1 in Fig. 8a), whose strength is 5 MPa lower than that of the rest of the model domain. We consider three different scenarios of fault weakening following a large fault rupture.

In the first scenario the fault zone is weakened instantly by 0.5 MPa immediately after the initial rupture, which has a stress drop of 1 MPa. This is the averaged stress drop in the fault zone of finite width (~70 km) and, thus, is lower than actual stress drops on the fault plane. The energy release of this rupture event is equivalent to an $M$ ~8 earthquake. Stress on the fault zone then gradually rises due to the far-field loading and viscous relaxation in the lower crust and the upper mantle (Fig. 9). When the stress in the fault zone reaches the new, lower fault strength in 1800 yr, a new rupture occurs

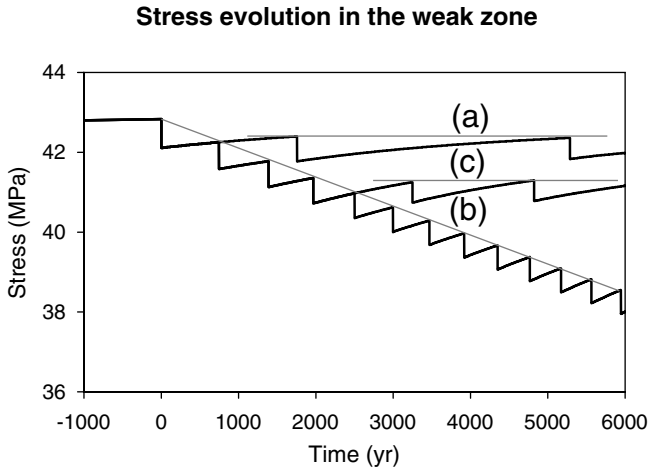


**Figure 9** Stress evolution in the weak zone with different weakening scenarios: (a) instant weakening, (b) continuous weakening, and (c) continuous weakening that stops after 2000 yr. Gray lines indicate the yield strength in each weakening scenario.

(Fig. 9). Assuming no further fault zone weakening, it then takes another 3000 yr for the fault zone to rupture again (Fig. 10a). The recurrence interval will be about one order of magnitude longer if the viscosity of lower crust and upper mantle is one order of magnitude higher ($> 10^{21}$ Pa sec).

In the second scenario, the fault zone continuously weakens at a rate of 1 MPa per 1000 yr after the first rupture. The stress in the weak zone recovers and is then released (Fig. 9) in a series of repeated earthquakes (Fig. 10b). The recurrence interval for the successive events is hundreds of years. Increasing the viscosity of lower crust and upper mantle increases little the recurrence interval because the recurrence interval is largely controlled by the speed of weakening.

In the third scenario, the fault zone gradually weakens in the first 2000 yr following the initial rupture. After that the fault zone maintains a constant strength. The stress evolution and rupture sequences in the first 2000 yr are the same as those in the second scenario. After the weakening stops, it takes a longer time for ruptures to repeat (Fig. 9). The recurrence interval is even longer if the viscosity of lower crust and upper mantle is higher. Eventually, the recurrence interval becomes long enough to be compatible with the rate of far-field boundary loading.

## Discussion

The spatiotemporal patterns of seismicity predicted by our simple model have some similarities to those observed in continental interiors. For a laterally homogeneous continent loaded mainly at its boundaries, as represented in our case 1, the seismicity is expected to align with the maximum shear stresses resulting from the loading conditions. In the simplest case the maximum compressive stress bisects conjugate trends of seismicity. However, this does not seem the case in the continents. The seismic belts in North China form conjugate north-northeast and southeast-east pairs (Fig. 1b), whereas the direction of present-day maximum compressive tectonic stress is around N55°E (Yuan *et al.*, 1999). The seismic belts in CEUS are oriented northeast (Fig. 1a), close to the average maximum compressive direction of tectonic stress of around N60°E (Zoback and Zoback, 1989). Thus, the orientation of seismic zones may instead be controlled by the inherited structures, such as ancient fault zones, which formed in a different stress field from the present one (Johnston and Schweig, 1996).

When significant weak zones are present in the crust, the model predicts that intraplate seismicity is not confined to these zones. Earthquakes occur all over, because the stress everywhere in the model domain is near its critical value for fault sliding. This condition is likely true for most continents where seismicity is broadly diffuse. Nonetheless, our results indicate that seismicity would concentrate along belts extending from the weak zones, oriented in the same directions as the weak zone and optimal failure directions.

The regional temporal clustering in the model (Fig. 7) is caused by coseismic and postseismic stress triggering. Such stress triggering may have caused a series of large earthquakes to occur on nearby faults within a short period, as

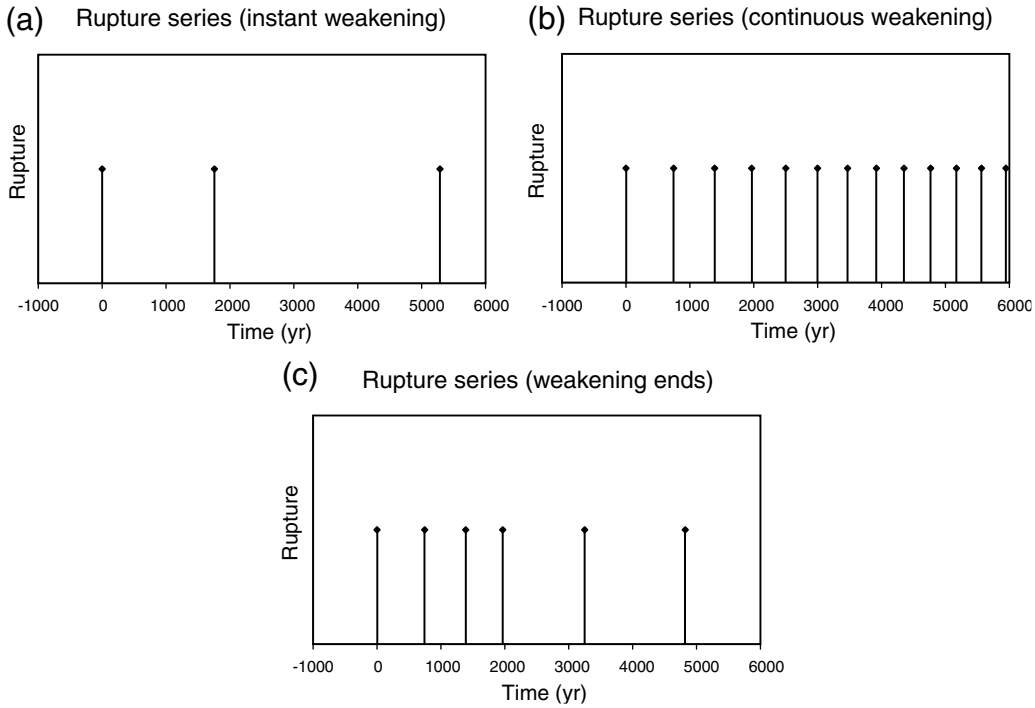


**Figure 10** Predicted crustal rupture sequences for (a) instant weakening, (b) continuous weakening, and (c) weakening that stops after 2000 yr.

in the 1811–1812 New Madrid seismic zone earthquakes (Mueller *et al.*, 2004) and the 2005–2007 Sumatra earthquakes (McCloskey *et al.*, 2005). However, our model cases 1 and 2, in which constant fault properties and tectonic loading are assumed, cannot explain repeated earthquakes on individual faults in short periods, such as the approximately 500 yr recurrence at the New Madrid seismic zone. Such repeated earthquakes on an individual fault may be predicted by the model if fault weakening is assumed (Fig. 10).

Although there is no direct evidence for fault weakening, several possible causes have been proposed. Sibson (1992) suggested fault weakening through change of water pore pressure on faults. Lyakhovsky *et al.* (2001) suggested changes of fault rheology due to a balance between weakening by earthquakes and interseismic healing. Fault weakening and healing may help to explain the paleoseismic data that have been interpreted to indicate for a series of large earthquakes in the New Madrid seismic zone with recurrence intervals of a few hundred years (Schweig and Ellis, 1994; Holbrook *et al.*, 2006). Kenner and Segall (2000) tried to simulate this inferred seismic sequence in a viscoelastic model. By assuming a sudden weakening of a localized weak lower crust embedded in an elastic crust, their model shows that weakening in the lower crust can causes stress amplification in the upper crust, resulting in a sequence of ruptures of the fault zone. Their predicted interseismic strain rate is below $1 \times 10^{-7}$ $\mathrm{yr}^{-1}$, below the detection level of previous Global Positioning System (GPS) surveys in the New Madrid seismic zone. Hence, the new zero crustal motion is indicated by the GPS data (Calais *et al.*, 2005; Smalley *et al.*, 2005). However, the cause of the sudden lower crust weakening is left for speculation. Alternatively, we have shown that the clusters of large intraplate earthquakes can result from fault weakening and healing, and the clusters can be separated by long periods of quiescence.

## Conclusions

We have explored the spatiotemporal patterns of intraplate earthquakes with a 3D finite-element model. The model includes far-field boundary loading, crustal failure in earthquakes, coseismic and postseismic stress evolution, and fault weakening. Our main results include the following:

1. Even with a horizontally homogeneous crust and mantle the model predicts complex spatiotemporal seismicity patterns that vary with timescales. Over hundreds of years the seismicity may appear both clustered in small belts and scattered over a larger region. Over thousands of years, the seismic clusters (belts) connect to form a network of seismic belts. Over tens of thousands of years, scattered seismicity covers the whole model region.
2. Coseismic and posterseismic triggering can cause temporal clustering of regional seismicity. If weak zones are incorporated in the model, the seismicity initiates in, but is not confined to, these zones.
3. Fault weakening can lead to repeated earthquakes on intraplate fault zones. The predicted temporal patterns of these repeated earthquakes vary with the weakening history.

Our model replicates some of the spatiotemporal complexity of clustered, episodic, and migrating intraplate earthquakes. Many factors not included in the model, such as a local driving force or that from the base of the lithosphere, and variable viscous rheology in the lower crust and upper mantle, may further contribute to the complexity of continental intraplate earthquakes. Our results of timescale-dependent spatiotemporal patterns of intraplate seismicity support the suggestions that seismicity patterns observed from short-term seismic records may not reflect the long-term patterns of intraplate seismicity (e.g., Crone *et al.*, 2003; Camelbeeck *et al.*, 2007). Because of the limited earthquake records in most places, assessment of earthquake hazard may be biased toward overestimating the hazard in regions of recent large earthquakes and underestimating the hazard where seismicity has been quiescent.

## Data and Resources

Seismicity data for the CEUS are from the National Earthquake Information Center (NEIC) catalog (http://neic.usgs.gov/neis/epic, last accessed June 2007). Earthquake data for North China are from China Earthquake Administration; these data may be obtained by contacting research scientist in the China Earthquake Administration.

## Acknowledgments

This work is partially supported by U.S. Geological Survey (USGS) Grant Number 04HQGR0046, National Science Foundation (NSF) Division of Earth Sciences (EAR) Grant Number 0225546, and NASA Cooperative Agreement Number NCC5-679. We thank Editor Fred Pollitz, Susan Hough, and an anonymous reviewer for their constructive comments.

## References

Calais, E., G. Mattioli, C. Demets, J. M. Nocquet, S. Stein, A. Newman, and P. Rydelek (2005). Tectonic strain in plate interiors?, *Nature* **438,** E9–E10.

Camelbeeck, T., K. Vanneste, P. Alexandre, K. Verbeeck, T. Petermans, P. Rosset, M. Everaerts, R. Warnant, and M. Van Camp (2007). Relevance of active faulting and seismicity studies to assess long term earthquake activity in Northwest Europe, in *Continental Intraplate Earthquakes: Science, Hazard, and Policy Issues*, S. Stein and S. Mazzotti (Editors), Special Paper 425, Geol. Soc. Am., Boulder, Colorado, 193–224.

Chéry, J., S. Merkel, and S. Bouissou (2001). A physical basis for time clustering of large earthquakes, *Bull. Seismol. Soc. Am.* **91,** 1685–1693.

Cisternas, M., B. F. Atwater, F. Torrejón, Y. Sawai, G. Machuca, M. Lagos, A. Eipert, C. Youlton, I. Salgado, T. Kamataki, M. Shishikura, C. P. Rajendran, J. K. Malik, Y. Rizal, and M. Husni (2005). Predecessors of the giant 1960 Chile earthquake, *Nature* **437,** 404–407.

Clark, D., and K. McCue (2003). Australian paleoseismology: towards a better basis for seismic hazard estimation, *Ann. Geophys.* **46,** 1087–1105.

Crone, A. J., and K. V. Luza (1990). Style and timing of Holocene surface faulting on the Meers fault, southwestern Oklahoma, *GSA Bull.* **102,** 1–17.

Crone, A. J., P. M. De Martini, M. N. Machette, K. Okumura, and J. R. Prescott (2003). Paleoseismicity of two historically quiescent faults in Australia: implications for fault behavior in stable continental regions, *Bull. Seismol. Soc. Am.* **93,** 1913–1934.

Gan, W., and W. H. Prescott (2001). Crustal deformation rates in central and eastern U.S. inferred from GPS, *Geophys. Res. Lett.* **28,** 3733–3736.

Hager, B. H. (Editor) (1991). *Mantle Viscosity: A Comparison of Models from Postglacial Rebound and from the Geoid, Plate Driving Forces, and Advected Heat Flux*, Kluwer Academic Publishers, London.

Halchuk, S., and J. Adams (1999). Crossing the border: assessing the differences between new Canadian and American seismic hazard maps, in *Proceedings Eighth Canadian Conference on Earthquake Engineering*, 77–82.

Holbrook, J., W. J. Autin, T. M. Rittenour, S. Marshak, and R. J. Goble (2006). Stratigraphic evidence for millennial-scale temporal clustering of earthquakes on a continental-interior fault: holocene Mississippi River floodplain deposits, New Madrid seismic zone, USA, *Tectonophysics* **420,** 431–454.

Johnston, A. C., and E. S. Schweig (1996). The enigma of the New Madrid earthquakes of 1811–1812, *Annu. Rev. Earth Planet. Sci.* **24,** 339–384.

Kenner, S. J., and P. Segall (2000). A mechanical model for intraplate earthquakes; application to the New Madrid seismic zone, *Science* **289,** 2329–2332.

Li, Q., and M. Liu (2006). Geometrical impact of the San Andreas fault on stress and seismicity in California, *Geophys. Res. Lett.* **33,** L08302, doi 08310.01029/02005GL025661.

Li, Q., and M. Liu (2007). Initiation of the San Jacinto fault and its interaction with the San Andreas fault: insights from geodynamic modeling, *Pure Appl. Geophys.* **164,** 1937–1945.

Li, Q., M. Liu, and E. Sandvol (2005). Stress evolution following the 1811–1812 large earthquakes in the New Madrid seismic zone, *Geophys. Res. Lett* **32,** L11310, doi 10.1029/2004GL022133.

Lyakhovsky, V., Y. Ben-Zion, and A. Agnon (2001). Earthquake cycle, fault zones, and seismicity patterns in a rheologically layered lithosphere, *J. Geophys. Res.* **106,** 4103–4120.

Marco, S., M. Stein, A. Agnon, and H. Ron (1996). Long term earthquake clustering: a 50,000 year paleoseismic record in the Dead Sea graben, *J. Geophys. Res.* **101,** 6179–6192.

McCloskey, J., S. S. Nalbant, and S. Steacy (2005). Indonesian earthquake: Earthquake risk from co-seismic stress, *Nature* **434**, 291–291.

McKenna, J., S. Stein, and C. Stein (2007). Is the New Madrid seismic zone hotter and weaker than its surroundings?, in *Continental Intraplate Earthquakes: Science, Hazard, and Policy Issues*, S. Stein and S. Mazzotti (Editors), Special Paper 425, Geol. Soc. Am., Boulder, Colorado, 167–175.

Mueller, K., S. E. Hough, and R. Bilham (2004). Analysing the 1811–1812 New Madrid earthquakes with recent instrumentally recorded aftershocks, *Nature* **429,** 284–288.

Newman, A., S. Stein, J. Weber, J. Engeln, A. Mao, and T. Dixon (1999). Slow deformation and lower seismic hazard at the New Madrid seismic zone, *Science* **284,** 619–621.

Pollitz, F. F., C. Wicks, and W. Thatcher (2001a). Mantle flow beneath a continental strike-slip fault; postseismic deformation after the 1999 Hector Mine earthquake, *Science* **293,** 1814–1818.

Pollitz, F. F., L. Kellogg, and R. Bürgmann (2001b). Sinking mafic body in a reactivated lower crust: a mechanism for stress concentration at the New Madrid seismic zone, *Bull. Seismol. Soc. Am.* **91,** 1882–1897.

Rundle, J. B., P. B. Rundle, A. Donnellan, P. Li, W. Klein, G. Morein, D. L. Turcotte, and L. Grant (2006). Stress transfer in earthquakes, hazard estimation and ensemble forecasting: inferences from numerical simulations, *Tectonophysics* **413,** 109–125.

Schulte, S. M., and W. D. Mooney (2005). An updated global earthquake catalogue for stable continental regions: reassessing the correlation with ancient rifts, *Geophys. J. Int.* **161**, 707–721.

Schweig, E. S., and M. A. Ellis (1994). Reconciling short recurrence intervals with minor deformation in the New Madrid seismic zone, *Science* **264,** 1308–1311.

Sibson, R. H. (1992). Implications of fault-valve behaviour for rupture nucleation and recurrence, *Tectonophysics* **211,** 283–293.

Smalley, R., M. A. Ellis, J. Paul, and R. B. Van Arsdale (2005). Space geodetic evidence for rapid strain rates in the New Madrid seismic zone of central USA, *Nature* **435,** 1088–1090.

Stein, R. S. (1999). The role of stress transfer in earthquake occurrence, *Nature* **402,** 605–609.

Stein, S. and J. T. Freymueller (Editors) (2002). *Plate Boundary Zones: Concepts and Approaches*, American Geophysical Union, Washington, D.C., 425 pp.

Stein, S. and S. Mazzotti (Editors) (2007). *Continental Intraplate Earthquakes: Science, Hazard, and Policy Issues*, Special Paper 425, Geol. Soc. Am., Boulder, Colorado.

Swafford, L., and S. Stein (2007). Limitations of the short earthquake record for seismicity and seismic hazard studies, in *Continental Intraplate Earthquakes: Science, Hazard, and Policy Issues*, S. Stein and S. Mazzotti (Editors), Special Paper 425, Geol. Soc. Am., Boulder, Colorado, 49–58.

Tóth, L., E. Győri, P. Mónus, and T. Zsíros (2006). Seismic hazard in the Pannonian region, in *The Adria Microplate: GPS Geodesy, Tectonics and Hazards*, N. Pinter, G. Gyula, J. Weber, S. Stein and D. Medak (Editors), Springer, Netherlands, 369–384.

Turcotte, D. L., and G. Schubert (1982). *Geodynamics: Applications of Continuum Physics to Geological Problems*, John Wiley & Sons, New York, 369–384.

Tuttle, M. P., E. S. Schweig, J. D. Sims, R. H. Lafferty, L. W. Wolf, and M. L. Haynes (2002). The earthquake potential of the New Madrid seismic zone, *Bull. Seismol. Soc. Am.* **92,** 2080–2089.

van Lanen, X., and W. D. Mooney (2007). Integrated geologic and geophysical studies of North American continental intraplate seismicity, in *Continental Intraplate Earthquakes: Science, Hazard, and Policy Issues*, S. Stein and S. Mazzotti (Editors), Special Paper 425, Geol. Soc. Am., Boulder, Colorado, 101–112.

Weldon, R., K. Scharer, T. Fumal, and G. Biasi (2004). Wrightwood and the earthquake cycle: what a long recurrence record tells us about how faults work, *GSA Today* **14,** 4–10.

Yuan, J., J. Xu, and S. Gao (1999). Inversion analysis of present tectonic stress field in North China region based on GPS data, *Geol. Sci. Tech. Inf.* **18,** 99–103.

Zoback, M. L., and M. D. Zoback (1989). Tectonic stress field of the continental United States, in *Geophysical Framework of the Continental United States*, L. C. Pakiser and W. D. Mooney (Editors), Geol. Soc. Am. Memoir, Vol. **172**, 523–539.

Lunar and Planetary Institute
Universities Space Research Association
3600 Bay Area Boulevard
Houston, Texas 77058
li@lpi.usra.edu
(Q.L.)

Department of Geological Sciences
University of Missouri
Columbia, Missouri 65211
(M.L.)

Department of Earth and Planetary Sciences
Northwestern University
Evanston, Illinois 60208
(S.S.)

Manuscript received 1 April 2008